Strain Rate Dependent Micro-Mechanical Composite Material Model for Finite Element Impact Simulation

Ala Tabiei[1] and Weitao Yi[2]
The Center of Excellence in DYNA3D Analysis
Aerospace Engineering and Engineering Mechanics Department
University of Cincinnati, OH 45221-0070, USA
&
Robert Goldberg[3]
NASA Glenn Research Center
Cleveland, OH 44135

Abstract

The present study aims at implementation of a strain rate dependent, non-linear, micro-mechanics material model for laminated, unidirectional polymer matrix composites into the explicit finite element code LSDYNA. The objective is to develop an accurate and simple micro-mechanical, rate dependent material model, which is computationally efficient. Within the model a representative volume cell is assumed. The stress-strain relation including rate dependent effects for the micro-model is derived for both shell elements and solid elements. Micro Failure Criterion (MFC) is presented for each material constituent and failure mode. The implemented model can deal with problems such as impact, crashworthiness, and failure analysis under quasi-static loads. The developed material model has a wide range of applications such as jet engine jackets, armor plates, and structural crashworthiness simulation. The deformation response of two representative composite materials with varying fiber orientation is presented using the described technique. The predicted results compare favorably to experimental values.

[1] Associate Professor
[2] Graduate Research Assistant
[3] Aerospace Engineer

Introduction

Composites have wide applications as structural members in land, air, and sea vehicles. The strain rate dependent mechanical behavior of fiber reinforced polymer composite materials is important for applications involving impact. These applications cover a wide range of situations such as crashworthiness and protective armors in air and space vehicles, and other applications. Metals are known to have a rate dependent deformation response. Polymeric composites also exhibit strain rate dependent deformation and failure. Significant amount of published literature show that the material properties and response of polymer matrix composites do vary with strain rates. A review of the literature can be found in Goldberg [1].

Most of the three dimensional material models presented in the literature for rate sensitivity of composites are empirical and consider the entire lamina to be rate sensitive [1]. It is known that some fibers are rate sensitive and some are not. Almost all matrix materials, on the other hand, are known to be strain rate sensitive. Therefore, when developing strain rate sensitive equations for composites care must be taken to separate the effect of the constituents on the composite. For this purpose, micro-mechanics equations, in which the effective behavior of the composite is computed based on the properties and response of the individual constituents, are most suitable for this application. Goldberg [1] has developed three-dimensional constitutive equations to model the nonlinear, strain rate dependent tensile deformation of polymers. The formulation is based on revising viscoplastic constitutive equations previously developed for metals. In the presented work the previously developed equations are adopted into the current micro-mechanical material model.

The objective of the present work is to develop a three dimensional model to provide a reasonable predictions of the deformation response of polymer matrix composites including strain rate effects. The material model can capture the nonlinear material behavior of composites due to strain softening. To perform structural analysis of composite materials using the nonlinear finite element code LS-DYNA, a standard interface has also been developed and presented. The finite element implementation is carried out for both shell and brick elements.

Micromechanics Based Composite Material Model

Tabiei and Chen [2] developed a micromechanical model to predict the mechanical behavior of unidirectional fiber reinforced composite materials. Several assumptions were made in the original micromechanics model. First, the fiber material is homogeneous and linearly elastic. Second, the matrix material is homogeneous and linearly elastic. Third, the fiber positioning in the matrix material is such that the resulting lamina material is macromechanically homogeneous with a linear elastic deformation behavior. Finally, there is a complete and strong bond at the interface of the constituent materials.

Shown in Figure 1 is the representative unit cell, which is an assumed geometry of the idealized composite. The unit cell is divided into three sub-cells; one sub-cell is fiber, denoted as f, and two matrix sub-cells, denoted as M_A and M_B, respectively. The three sub-cells are grouped into two parts. Material Part A consists of the fiber sub-cell f and the series-or-parallel connected matrix sub-cell M_A. Material Part B consists of the remaining matrix M_B. The dimensions of the unit cell are 1x1 unit square. The dimensions of fiber and matrix sub-cells are denoted by W_f and W_m respectively as shown in Figure 1 and defined as below:

$$W_f = \sqrt{V_f}$$
$$W_m = 1 - W_f \qquad (1)$$

where V_f is the Fiber Volume Fraction. The effective stresses and strains in the lamina are determined from the sub-cell values in two phases: first, fiber f and matrix M_A construct Part A;

then Part A and Part B construct the unidirectional lamina. The homogenized stresses and strains in Part A are given by the following equations:

$$\begin{Bmatrix} \varepsilon_{11} \\ \sigma_{22} \\ \sigma_{33} \\ \sigma_{12} \\ \sigma_{23} \\ \sigma_{13} \end{Bmatrix}_A = \begin{Bmatrix} \varepsilon_{11} \\ \sigma_{22} \\ \sigma_{33} \\ \sigma_{12} \\ \sigma_{23} \\ \sigma_{13} \end{Bmatrix}_f = \begin{Bmatrix} \varepsilon_{11} \\ \sigma_{22} \\ \sigma_{33} \\ \sigma_{12} \\ \sigma_{23} \\ \sigma_{13} \end{Bmatrix}_{MA} \tag{2}$$

$$\begin{Bmatrix} \sigma_{11} \\ \varepsilon_{22} \\ \varepsilon_{33} \\ \varepsilon_{12} \\ \varepsilon_{23} \\ \varepsilon_{13} \end{Bmatrix}_A = W_f \begin{Bmatrix} \sigma_{11} \\ \varepsilon_{22} \\ \varepsilon_{33} \\ \varepsilon_{12} \\ \varepsilon_{23} \\ \varepsilon_{13} \end{Bmatrix}_f + W_m \begin{Bmatrix} \sigma_{11} \\ \varepsilon_{22} \\ \varepsilon_{33} \\ \varepsilon_{12} \\ \varepsilon_{23} \\ \varepsilon_{13} \end{Bmatrix}_{MA} \tag{3}$$

The homogenized stresses and strains in the unit cell are given by the following equations:

$$\begin{Bmatrix} \varepsilon_{11} \\ \varepsilon_{22} \\ \varepsilon_{33} \\ \varepsilon_{12} \\ \varepsilon_{23} \\ \varepsilon_{13} \end{Bmatrix}_C = \begin{Bmatrix} \varepsilon_{11} \\ \varepsilon_{22} \\ \varepsilon_{33} \\ \varepsilon_{12} \\ \varepsilon_{23} \\ \varepsilon_{13} \end{Bmatrix}_B = \begin{Bmatrix} \varepsilon_{11} \\ \varepsilon_{22} \\ \varepsilon_{33} \\ \varepsilon_{12} \\ \varepsilon_{23} \\ \varepsilon_{13} \end{Bmatrix}_A \tag{4}$$

$$\begin{Bmatrix} \sigma_{11} \\ \sigma_{22} \\ \sigma_{33} \\ \sigma_{12} \\ \sigma_{23} \\ \sigma_{13} \end{Bmatrix}_C = W_f \begin{Bmatrix} \sigma_{11} \\ \sigma_{22} \\ \sigma_{33} \\ \sigma_{12} \\ \sigma_{23} \\ \sigma_{13} \end{Bmatrix}_A + W_m \begin{Bmatrix} \sigma_{11} \\ \sigma_{22} \\ \sigma_{33} \\ \sigma_{12} \\ \sigma_{23} \\ \sigma_{13} \end{Bmatrix}_B \tag{5}$$

Part B is a homogeneous isotropic matrix (resin) material. The stiffness matrix is given by the following:

$$[Q]_B = [S]_B^{-1} = \begin{Bmatrix} \frac{E_m}{1-\nu_m^2} & \frac{\nu_m E_m}{1-\nu_m^2} & \frac{\nu_m E_m}{1-\nu_m^2} & 0 & 0 & 0 \\ \frac{\nu_m E_m}{1-\nu_m^2} & \frac{E_m}{1-\nu_m^2} & \frac{\nu_m E_m}{1-\nu_m^2} & 0 & 0 & 0 \\ \frac{\nu_m E_m}{1-\nu_m^2} & \frac{\nu_m E_m}{1-\nu_m^2} & \frac{E_m}{1-\nu_m^2} & 0 & 0 & 0 \\ 0 & 0 & 0 & G_m & 0 & 0 \\ 0 & 0 & 0 & 0 & G_m & 0 \\ 0 & 0 & 0 & 0 & 0 & G_m \end{Bmatrix}_B \tag{6}$$

The total stress is obtained from the following:

$$\{\sigma\}_B = [Q]_B \cdot \{\varepsilon\}_B \tag{7}$$

Part A consists of an isotropic matrix sub-cell M_A and an orthotropic fiber sub-cell f. The stifness matrix for M_A is given by the following equation:

$$[Q]_{MA} = [S]_{MA}^{-1} = \begin{Bmatrix} \frac{E_m}{1-\nu_m^2} & \frac{\nu_m E_m}{1-\nu_m^2} & \frac{\nu_m E_m}{1-\nu_m^2} & 0 & 0 & 0 \\ \frac{\nu_m E_m}{1-\nu_m^2} & \frac{E_m}{1-\nu_m^2} & \frac{\nu_m E_m}{1-\nu_m^2} & 0 & 0 & 0 \\ \frac{\nu_m E_m}{1-\nu_m^2} & \frac{\nu_m E_m}{1-\nu_m^2} & \frac{E_m}{1-\nu_m^2} & 0 & 0 & 0 \\ 0 & 0 & 0 & G_m & 0 & 0 \\ 0 & 0 & 0 & 0 & G_m & 0 \\ 0 & 0 & 0 & 0 & 0 & G_m \end{Bmatrix}_{MA} \tag{8}$$

The total stress is obtained from the following:

$$\{\sigma\}_{M_A} = [Q]_{M_A} \cdot \{\varepsilon\}_{M_A} \tag{9}$$

Sub-cell f is the fiber portion of the unit cell and the stiffness matrix is given by the following equation:

$$[Q]_f = [S]_f^{-1} = \begin{Bmatrix} \frac{1}{E_2^f E_f} & \frac{\nu_f}{E_1^f E_f} & \frac{\nu_f}{E_1^f E_f} & 0 & 0 & 0 \\ \frac{\nu_f}{E_1^f E_f} & \frac{\nu_f}{E_1^f E_f} & \frac{\nu_f}{E_1^f E_f} & 0 & 0 & 0 \\ \frac{\nu_f}{E_1^f E_f} & \frac{\nu_f}{E_1^f E_f} & \frac{\nu_f}{E_1^f E_f} & 0 & 0 & 0 \\ 0 & 0 & 0 & G_{12}^f & 0 & 0 \\ 0 & 0 & 0 & 0 & G_{23}^f & 0 \\ 0 & 0 & 0 & 0 & 0 & G_{23}^f \end{Bmatrix}_f \tag{10}$$

where $E_f = \frac{1}{E_1^f E_2^f} - \frac{{\nu_f}^2}{{E_1^f}^2}$

The total stress is obtained from the following:

$$\{\sigma\}_f = [Q]_f \cdot \{\varepsilon\}_f \tag{11}$$

So, finally for Part A, we have the following:

$$\begin{Bmatrix} \sigma_{22} \\ \sigma_{33} \\ \sigma_{12} \\ \sigma_{23} \\ \sigma_{13} \end{Bmatrix}_A = \begin{Bmatrix} \sigma_{22} \\ \sigma_{33} \\ \sigma_{12} \\ \sigma_{23} \\ \sigma_{13} \end{Bmatrix}_f = \begin{Bmatrix} \sigma_{22} \\ \sigma_{33} \\ \sigma_{12} \\ \sigma_{23} \\ \sigma_{13} \end{Bmatrix}_{M_A} \tag{12}$$

$$\{\sigma_{11}\}_A = W_f \{\sigma_{11}\}_f + W_m \{\sigma_{11}\}_{M_A} \tag{13}$$

The total stresses for unit cell are finally obtained from the following:

$$\begin{Bmatrix}\sigma_{22}\\ \sigma_{33}\\ \sigma_{12}\\ \sigma_{23}\\ \sigma_{13}\end{Bmatrix}_C = W_f \begin{Bmatrix}\sigma_{22}\\ \sigma_{33}\\ \sigma_{12}\\ \sigma_{23}\\ \sigma_{13}\end{Bmatrix}_A + W_m \begin{Bmatrix}\sigma_{22}\\ \sigma_{33}\\ \sigma_{12}\\ \sigma_{23}\\ \sigma_{13}\end{Bmatrix}_B \tag{14}$$

Strain Rate Effects

As previously described, the rate dependency of composite materials is primarily a function of the rate dependency of the matrix constituent, particularly for carbon fiber reinforced composites. There are rate sensitive fibers like Boron and others, but in this study only the matrix material is assumed to be rate sensitive. Furthermore, the stress-strain response of the matrix is assumed to be nonlinear.

The Ramaswamy-Stouffer viscoplastic state variable model [3], which was originally developed to analyze the viscoplastic deformation of metals above one-half of the melting temperature, has been modified to simulate the rate dependent inelastic deformation of a ductile polymer. As discussed in reference [1], there is some physical motivation in utilizing constitutive equations that were developed for viscoplastic metals to analyze the deformation response of ductile polymers. In state variable constitutive equations, a single unified strain variable is defined to represent all inelastic strains. Furthermore, there is no defined yield stress. Inelastic strains are assumed to be present at all values of stress, only very small in the "elastic" range of deformation. State variables, which evolve with stress and inelastic strain, are defined to represent the average effects of the deformation mechanisms.

Several limitations and assumptions have been specified in the development of the constitutive equations. Small strain conditions are assumed and temperature effects are neglected. The nonlinear strain recovery observed in polymers on unloading is not simulated, and phenomena such as creep, relaxation and high cycle fatigue are not accounted for in the equations.

In the modified Ramaswamy-Stouffer model, the inelastic strain rate, $\dot{\varepsilon}_{ij}^{I}$, is defined as a function of the deviatoric stress, s_{ij}, and tensorial internal stress state variable Ω_{ij} in the form

$$\dot{\varepsilon}_{ij}^{I} = D_o \exp\left[-\frac{1}{2}\left(\frac{Z_o^2}{3K_2}\right)^n\right]\left(\frac{s_{ij}-\Omega_{ij}}{\sqrt{K_2}}\right) \tag{15}$$

where D_o, Z_o, and n are material constants. The term K_2 is defined as follows

$$K_2 = \frac{1}{2}\left(s_{ij}-\Omega_{ij}\right)\left(s_{ij}-\Omega_{ij}\right) \tag{16}$$

and represents the second invariant of the overstress tensor. The elastic components of strain are added to the inelastic strain to obtain the total strain. The following relation defines the internal stress variable rate

$$\dot{\Omega}_{ij} = \frac{2}{3} q\Omega_m \dot{\varepsilon}_{ij}^{I} - q\Omega_{ij}\dot{\varepsilon}_e^{I} \tag{17}$$

where q is a material constant, Ω_m is a material constant that represents the maximum value of the internal stress, and ε_e^{I} is the effective inelastic strain. The material constants are determined in the manner discussed in references [1] and [3].

Bordonaro [4] indicated that the proper way to account for hydrostatic stresses in polymers in a state variable constitutive model was to modify the effective stress terms. In this work,

pressure dependence is included by multiplying the shear terms in the K_2 invariant in Equation 16 by the following correction factor

$$\alpha = \left(\frac{\sigma_m}{\sqrt{J_2}} \right)^{\beta} \tag{18}$$

where σ_m is the mean stress, J_2 is the second invariant of the deviatoric stress tensor, and β is a material constant. The value of the parameter β is currently determined empirically by fitting data from uniaxial composites with shear dominated fiber orientations, such as $[\pm 45°]_s$.

The resin constitutive equations and the composite micromechanics model described in [2] have been implemented into the dynamic explicit finite element code LS-DYNA as a user-defined material subroutine. In previous work [1,5], an alternative mechanics of materials based micromechanics method was utilized to predict the strain rate dependent, nonlinear deformation response of polymer matrix composites. However, by implementing the resin constitutive equations into the micromechanics model presented in this study, the flexibility of the constitutive equations can be demonstrated. Furthermore, the analyses presented in references [1] and [5] did not incorporate the micro failure criteria presented here, which provides for a more accurate prediction of the constituent based failure of the composite. For implementation in LS-DYNA, the polymer constitutive equations must be converted into an incremental format. To convert the flow equation (Equation (15)) into an incremental form, the rate equation is multiplied by the time increment dt of the current time step to compute the inelastic strain increment $d\varepsilon_{ij}^I$. The resulting equation is as follows:

$$d\varepsilon_{ij}^I = D_o \exp\left[-\frac{1}{2}\left(\frac{Z_o^2}{3K_2} \right)^n \right] * \frac{s_{ij} - \Omega_{ij}}{\sqrt{K_2}} * dt \tag{19}$$

where all of the terms are as defined earlier. Note that the total value of the deviatoric stress components and the internal stress components are used instead of the stress increments, and are the values from the previous time step. Equations (17) and (18) are modified to compute the increment in internal stress, $d\Omega_{ij}$, and the increment in effective inelastic strain, $d\varepsilon_e^I$. The following equations result

$$d\Omega_{ij} = \frac{2}{3} q\Omega_m d\varepsilon_{ij}^I - q\Omega_{ij} d\varepsilon_e^I \tag{20}$$

$$d\varepsilon_e^I = \sqrt{\frac{2}{3} d\varepsilon_{ij}^I d\varepsilon_{ij}^I} \tag{21}$$

and all the terms in the equations are as defined earlier. In Equation (20), the total value of the internal stress from the previous time increment is used in computing the stress increment for the current time step.

The equations and the micromechanics equations described earlier were used to compute the rate dependent, inelastic response of the polymer matrix composite. Considering the nonlinearity and strain rate dependence present in the resin, the incremental stresses in the micromechanics model are modified to following new form:
The stresses in subcell B are:

$$d\sigma_{11b} = \frac{E_m}{1 - \nu_m^2} [(d\varepsilon_{11} - d\varepsilon_{11}^I) + (d\varepsilon_{22} - d\varepsilon_{22}^I + d\varepsilon_{33} - d\varepsilon_{33}^I) \cdot \nu_m] \tag{22}$$

$$d\sigma_{22b} = \frac{E_m}{1 - \nu_m^2} [(d\varepsilon_{22} - d\varepsilon_{22}^I) + (d\varepsilon_{11} - d\varepsilon_{11}^I + d\varepsilon_{33} - d\varepsilon_{33}^I) \cdot \nu_m] \tag{23}$$

$$d\sigma_{33b} = \frac{E_m}{1-\nu_m^2}[(d\varepsilon_{33} - d\varepsilon_{33}^I) + (d\varepsilon_{11} - d\varepsilon_{11}^I + d\varepsilon_{22} - d\varepsilon_{22}^I)\cdot \nu_m] \quad (24)$$

$$d\sigma_{12b} = (d\varepsilon_{12} - d\varepsilon_{12}^I)\cdot G_m \quad (25)$$

$$d\sigma_{13b} = (d\varepsilon_{13} - d\varepsilon_{13}^I)\cdot G_m \quad (26)$$

$$d\sigma_{12b} = (d\varepsilon_{23} - d\varepsilon_{23}^I)\cdot G_m \quad (27)$$

The stresses in subcell A are:

$$d\sigma_{11a} = (d\varepsilon_{11} - d\varepsilon_{11}^I)\cdot E_m + d\sigma_{22a}\cdot \nu_m \quad (28)$$

$$d\sigma_{22a} = E_{12m}\cdot[(d\varepsilon_{22} - d\varepsilon_{22}^I) + (W_f\cdot\nu_f + W_m\cdot\nu_m)\cdot(d\varepsilon_{11} - d\varepsilon_{11}^I + d\varepsilon_{33} - d\varepsilon_{33}^I)] \quad (29)$$

$$d\sigma_{33a} = E_{12m}\cdot[(d\varepsilon_{33} - d\varepsilon_{33}^I) + (W_f\cdot\nu_f + W_m\cdot\nu_m)\cdot(d\varepsilon_{11} - d\varepsilon_{11}^I + d\varepsilon_{22} - d\varepsilon_{22}^I)] \quad (30)$$

$$d\sigma_{12a} = \frac{d\varepsilon_{12} - d\varepsilon_{12}^I}{\frac{W_f}{G_{12}^f} + \frac{W_m}{G_m}} \quad (31)$$

$$d\sigma_{13a} = \frac{d\varepsilon_{13} - d\varepsilon_{13}^I}{\frac{W_f}{G_{23}^f} + \frac{W_m}{G_m}} \quad (32)$$

$$d\sigma_{23a} = \frac{d\varepsilon_{23} - d\varepsilon_{23}^I}{\frac{W_f}{G_{23}^f} + \frac{W_m}{G_m}} \quad (33)$$

$$d\sigma_{11f} = d\varepsilon_{11}\cdot E_1^f + d\sigma_{22a}\cdot\nu_f \quad (34)$$

where

$$E_{12m} = \frac{E_1^f\cdot E_2^f\cdot E_m}{[E_m\cdot W_f\cdot(E_1^f - E_2^f\cdot\nu_f^2) + E_1^f\cdot E_2^f\cdot W_m\cdot(1-\nu_m^2)]} \quad (35)$$

The failure analysis is carried out by comparing the stresses or strains with those permissible values of stresses or strains of the constituents. At every increment of the applied stress, the stresses (or strains) are monitored for failure. Property degradation models are utilized. For structural level modeling, the ability to only degrade certain material properties based on the local ply failure mechanisms is desirable to provide improved simulation of the stress transfer mechanisms. Furthermore, in implementing the model into the finite element code, a gradual degradation of material properties improves the stability of the finite element analysis. In this study, stresses are decreased to zero in 100 steps if failure happens.

Failure Analysis

Simple failure models for composite materials can be used to reliably predict the onset of failure, but not to predict the post-failure deformation, which are important in the impact analysis [6]. Complex composite damage models must be developed which account for a combination of several typical failure mechanisms: transverse matrix cracking, transverse matrix crushing, fiber breakage, fiber buckling, and matrix crashing in the fiber direction. These failure modes can be accounted for by employing micro-mechanical failure criteria (MFC) to model the progressive damage in the laminae.

When failure occurs, the material will lose its load carrying capability in certain modes of deformation. To adequately model this behavior, the compliance matrix and stresses are

modified according to the failure modes. To simulate failure in the explicit finite element method, failure must be modeled by a gradual loss of stiffness in order to provide a stable solution instead of an instantaneous loss. A transition to the failed condition is assumed to occur during a finite time. The micro failure criteria used in the model are as follows:

Fiber Fracture in Tension

A unidirectional lamina subjected to tensile loading in the fiber direction may fail by fiber fracture. Failure is determined by the tensile strength of the fiber when $\sigma_{11}^f \geq X_t^f$, if this occurs, the fiber compliance matrix is degraded as follows:

$$[S]_f = \begin{bmatrix} \frac{1}{E_1^f} & -\frac{\nu_f}{E_1^f} & -\frac{\nu_f}{E_1^f} & 0 & 0 & 0 \\ -\frac{\nu_f}{E_1^f} & \frac{1}{E_2^f} & -\frac{\nu_f}{E_1^f} & 0 & 0 & 0 \\ -\frac{\nu_f}{E_1^f} & -\frac{\nu_f}{E_1^f} & \frac{1}{E_2^f} & 0 & 0 & 0 \\ 0 & 0 & 0 & \frac{1}{G_{12}^f} & 0 & 0 \\ 0 & 0 & 0 & 0 & \frac{1}{G_{23}^f} & 0 \\ 0 & 0 & 0 & 0 & 0 & \frac{1}{G_{23}^f} \end{bmatrix} \Rightarrow \begin{bmatrix} D_1^{-1}\frac{1}{E_1^f} & 0 & 0 & 0 & 0 & 0 \\ 0 & \frac{1}{E_2^f} & 0 & 0 & 0 & 0 \\ 0 & 0 & \frac{1}{E_2^f} & 0 & 0 & 0 \\ 0 & 0 & 0 & \frac{1}{G_{12}^f} & 0 & 0 \\ 0 & 0 & 0 & 0 & \frac{1}{G_{23}^f} & 0 \\ 0 & 0 & 0 & 0 & 0 & \frac{1}{G_{23}^f} \end{bmatrix}$$

where D_1 is the stiffness reduction factor, which serves to degrade the fiber axial stiffness. Since the tensile fiber fracture failure corresponds to the opening of cracks, the axial stress in the fiber is also relieved, $\sigma_{11}^f = 0$.

Matrix Cracking in Axial Tension

Although this damage mechanism is not a very serious damage mode, its consideration may be warranted in composites with low fiber volume fraction. Failure is determined by the tensile strength of the matrix when $\max(\sigma_{11}^{M_A}, \sigma_{11}^B) \geq Y_t^m$, if this occurs, the resin compliance matrix is degraded as follows:

$$[S]_{M_A,B} = \begin{bmatrix} \frac{1}{E_m} & -\frac{\nu_m}{E_m} & -\frac{\nu_m}{E_m} & 0 & 0 & 0 \\ -\frac{\nu_m}{E_m} & \frac{1}{E_m} & -\frac{\nu_m}{E_m} & 0 & 0 & 0 \\ -\frac{\nu_m}{E_m} & -\frac{\nu_m}{E_m} & \frac{1}{E_m} & 0 & 0 & 0 \\ 0 & 0 & 0 & \frac{1}{G_m} & 0 & 0 \\ 0 & 0 & 0 & 0 & \frac{1}{G_m} & 0 \\ 0 & 0 & 0 & 0 & 0 & \frac{1}{G_m} \end{bmatrix} \Rightarrow \begin{bmatrix} D_2^{-1}\frac{1}{E_m} & 0 & 0 & 0 & 0 & 0 \\ 0 & \frac{1}{E_m} & 0 & 0 & 0 & 0 \\ 0 & 0 & \frac{1}{E_m} & 0 & 0 & 0 \\ 0 & 0 & 0 & \frac{1}{G_m} & 0 & 0 \\ 0 & 0 & 0 & 0 & \frac{1}{G_m} & 0 \\ 0 & 0 & 0 & 0 & 0 & \frac{1}{G_m} \end{bmatrix}$$

where D_2 is the stiffness reduction factor, which serves to degrade the matrix axial stiffness. Since this is a tensile matrix crack failure, the axial stress in the matrix is also relieved, $\sigma_{11}^{M_A}, \sigma_{11}^{B} = 0$.

Matrix Cracking in Transverse Tension

This damage mode is determined by the tensile strength of the matrix when $\max(\sigma_{22}^{M_A}, \sigma_{22}^{B}) \geq Y_t^m$, if this occurs, the resin compliance matrix is degraded as follows:

$$[S]_{M_A,B} = \begin{bmatrix} \frac{1}{E_m} & -\frac{\nu_m}{E_m} & -\frac{\nu_m}{E_m} & 0 & 0 & 0 \\ -\frac{\nu_m}{E_m} & \frac{1}{E_m} & -\frac{\nu_m}{E_m} & 0 & 0 & 0 \\ -\frac{\nu_m}{E_m} & -\frac{\nu_m}{E_m} & \frac{1}{E_m} & 0 & 0 & 0 \\ 0 & 0 & 0 & \frac{1}{G_m} & 0 & 0 \\ 0 & 0 & 0 & 0 & \frac{1}{G_m} & 0 \\ 0 & 0 & 0 & 0 & 0 & \frac{1}{G_m} \end{bmatrix} \Rightarrow \begin{bmatrix} \frac{1}{E_m} & -\frac{\nu_m}{E_m} & -\frac{\nu_m}{E_m} & 0 & 0 & 0 \\ -\frac{\nu_m}{E_m} & D_3^{-1}\frac{1}{E_m} & -\frac{\nu_m}{E_m} & 0 & 0 & 0 \\ -\frac{\nu_m}{E_m} & -\frac{\nu_m}{E_m} & \frac{1}{E_m} & 0 & 0 & 0 \\ 0 & 0 & 0 & D_4^{-1}\frac{1}{G_m} & 0 & 0 \\ 0 & 0 & 0 & 0 & \frac{1}{G_m} & 0 \\ 0 & 0 & 0 & 0 & 0 & \frac{1}{G_m} \end{bmatrix}$$

where D_3, D_4 *are* the stiffness reduction factor which serves to degrade the matrix stiffness in the transverse direction and in-plane shear respectively. Since we have opening of cracks, the transverse direction stress in the matrix is also relieved, $\sigma_{22}^{M_A}, \sigma_{22}^{B} = 0$. In addition, since the stresses in matrix subcell M_A are related to the stress in the fiber, the $\sigma_{22}^{(f)}$ is also reduced to zero, $\sigma_{22}^{f} = 0$.

Matrix Crush in Transverse Compression

This is assumed to be a result of compressive failure of the matrix material. Failure is determined by the compressive strength of the matrix when $\max(|\sigma_{22}^{M_A}|, |\sigma_{22}^{B}|) \geq Y_c^m$, if this occurs, the resin compliance matrix is degraded as follows:

$$[S]_{M_A,B} = \begin{bmatrix} \frac{1}{E_m} & -\frac{\nu_m}{E_m} & -\frac{\nu_m}{E_m} & 0 & 0 & 0 \\ -\frac{\nu_m}{E_m} & \frac{1}{E_m} & -\frac{\nu_m}{E_m} & 0 & 0 & 0 \\ -\frac{\nu_m}{E_m} & -\frac{\nu_m}{E_m} & \frac{1}{E_m} & 0 & 0 & 0 \\ 0 & 0 & 0 & \frac{1}{G_m} & 0 & 0 \\ 0 & 0 & 0 & 0 & \frac{1}{G_m} & 0 \\ 0 & 0 & 0 & 0 & 0 & \frac{1}{G_m} \end{bmatrix} \Rightarrow \begin{bmatrix} D_2^{-1}\frac{1}{E_m} & 0 & 0 & 0 & 0 & 0 \\ 0 & \frac{1}{E_m} & 0 & 0 & 0 & 0 \\ 0 & 0 & \frac{1}{E_m} & 0 & 0 & 0 \\ 0 & 0 & 0 & \frac{1}{G_m} & 0 & 0 \\ 0 & 0 & 0 & 0 & \frac{1}{G_m} & 0 \\ 0 & 0 & 0 & 0 & 0 & \frac{1}{G_m} \end{bmatrix}$$

where D_2 is the stiffness reduction factor, which serves to degrade the matrix axial stiffness. The stress in the matrix is not relieved.

In Plane Matrix Shearing

This damage mode is determined by the tensile strength of the matrix when $\max(|\tau_{12}^{M_A}|,|\tau_{12}^{B}|) \geq S^m$, if this occurs, the resin compliance matrix is degraded as follows:

$$[S]_{M_A,B} = \begin{bmatrix} \frac{1}{E_m} & -\frac{\nu_m}{E_m} & -\frac{\nu_m}{E_m} & 0 & 0 & 0 \\ -\frac{\nu_m}{E_m} & \frac{1}{E_m} & -\frac{\nu_m}{E_m} & 0 & 0 & 0 \\ -\frac{\nu_m}{E_m} & -\frac{\nu_m}{E_m} & \frac{1}{E_m} & 0 & 0 & 0 \\ 0 & 0 & 0 & \frac{1}{G_m} & 0 & 0 \\ 0 & 0 & 0 & 0 & \frac{1}{G_m} & 0 \\ 0 & 0 & 0 & 0 & 0 & \frac{1}{G_m} \end{bmatrix} \Rightarrow \begin{bmatrix} \frac{1}{E_m} & -\frac{\nu_m}{E_m} & -\frac{\nu_m}{E_m} & 0 & 0 & 0 \\ -\frac{\nu_m}{E_m} & D_3^{-1}\frac{1}{E_m} & -\frac{\nu_m}{E_m} & 0 & 0 & 0 \\ -\frac{\nu_m}{E_m} & -\frac{\nu_m}{E_m} & \frac{1}{E_m} & 0 & 0 & 0 \\ 0 & 0 & 0 & D_4^{-1}\frac{1}{G_m} & 0 & 0 \\ 0 & 0 & 0 & 0 & \frac{1}{G_m} & 0 \\ 0 & 0 & 0 & 0 & 0 & \frac{1}{G_m} \end{bmatrix}$$

where D_3, D_4 is the stiffness reduction factor which serves to degrade the matrix stiffness in transverse direction and in-plane shearing. No stress relieving is carried out.

Matrix Shearing In Transverse Directions

Matrix cracking in the transverse shear direction occurs when the max of $(|\sigma_{13}^{m_A}|,|\sigma_{13}^{m_B}|)$ or $(|\sigma_{23}^{m_A}|,|\sigma_{23}^{m_B}|)$ is greater than the shear strength of the matrix material. If this occurs, the resin compliance matrix is degraded as follows:

$$[S]_{M_A,B} = \begin{bmatrix} \frac{1}{E_m} & -\frac{\nu_m}{E_m} & -\frac{\nu_m}{E_m} & 0 & 0 & 0 \\ -\frac{\nu_m}{E_m} & \frac{1}{E_m} & -\frac{\nu_m}{E_m} & 0 & 0 & 0 \\ -\frac{\nu_m}{E_m} & -\frac{\nu_m}{E_m} & \frac{1}{E_m} & 0 & 0 & 0 \\ 0 & 0 & 0 & \frac{1}{G_m} & 0 & 0 \\ 0 & 0 & 0 & 0 & \frac{1}{G_m} & 0 \\ 0 & 0 & 0 & 0 & 0 & \frac{1}{G_m} \end{bmatrix} \Rightarrow \begin{bmatrix} \frac{1}{E_m} & -\frac{\nu_m}{E_m} & -\frac{\nu_m}{E_m} & 0 & 0 & 0 \\ -\frac{\nu_m}{E_m} & \frac{1}{E_m} & -\frac{\nu_m}{E_m} & 0 & 0 & 0 \\ -\frac{\nu_m}{E_m} & -\frac{\nu_m}{E_m} & \frac{1}{E_m} & 0 & 0 & 0 \\ 0 & 0 & 0 & \frac{1}{G_m} & 0 & 0 \\ 0 & 0 & 0 & 0 & D_5^{-1}\frac{1}{G_m} & 0 \\ 0 & 0 & 0 & 0 & 0 & D_5^{-1}\frac{1}{G_m} \end{bmatrix}$$

where D_5 is the stiffness reduction factor which serves to degrade the matrix shear stiffness in transverse direction. No stress relieving is carried out.

Lamina Failure by Kink-banding

In axial compression, the failure is assumed to be triggered by fiber micro-buckling which results in kink-banding. Several analytical models for the prediction of compressive strength have not shown good quantitative agreement with experimental results, but they served to identify the important parameters affecting the compressive strength of unidirectional composites which

appear to be the matrix shear modulus, fiber misalignment, fiber diameter, fiber volume fraction, and fiber/matrix interface strength.

Here, modified strength criteria suggested by Hahn and Williams [7] is used ($\sigma_{crit} = V_f G_{12}^{La\min te}$), where G_{12} is the in-plane shear modulus of the lamina. In the present analysis, kink-banding is assumed to occur if $|\sigma_{11}|_{La\min a} \geq \sigma_{crit}$, and the stiffness of the constituents are reduced; but no stress relieving.

Numerical Results

As demonstration of the ability of the developed rate dependent micro-mechanical material model in the prediction of rate effects of composites several examples are considered and discussed in this section. One example considers a series of plates modeled using shell and solid elements under different rates of loading. The material considered in this example is an AS4/PEEK composite material under various rates of tensile loading. The second example considered here is the crashworthiness of an Eglass/Epoxy tube under axial impact. The final example considered is a perforation of composite armor by a high velocity object.

1. AS4/PEEK tensile loading simulation:

PEEK (polyetheretherketone) is a thermoplastic material, and AS4 is a carbon fiber. The material properties for the examples are listed here. The fiber volume ratio used for the AS4/PEEK material is 0.62. Table 1 presents the material properties of the AS4 fiber tows, and Table 2 presents the material properties of PEEK resin. Note that there is no failure in this example due to the small strain. Both four noded shell elements and eight noded solid elements were used in a square mesh. Each side of the model is 20 mm long, and the thickness is 2mm. The left hand side of the model was clamped, and a constantly increasing specified displacement is applied to the right hand side of the model.

where the variables are as defined in previous sections. The material constants were determined using the procedures specified in references [1] and [3]. As a reminder, the value of the parameter β was correlated based on macroscopic results from a composite with a shear dominated fiber orientation.

The predicted results were compared to experimentally obtained values obtained by Weeks and Sun [8]. During the analysis, unidirectional laminates with fiber orientations of [15°], [30°] and [45°] are considered. Comparisons between prediction result and experimental data are shown in Figure (2-4) for a strain rate of 0.1/sec, using shell elements. As can be seen in the figures, qualitatively the nonlinearity of the deformation response is captured, and quantitatively the analytical results match the experimental values reasonably well in general for all fiber orientation angles examined.

To examine the ability of the methodology to capture the rate dependence of the composite response, plots of stress-strain curves for different strain rates, which are 0.1/sec, 0.01/sec and 0.001/sec, using shell elements, are shown in Figure (5-7) for the fiber orientation angles examined above. Figures 8 and 9 present the stress-strain curves for different strain rates, which are 1/sec, 0.1/sec and 0.01/sec, using solid elements. The fiber orientations examined here are [30°] and [45°]. For both element types and for all fiber orientations examined, the analysis predicts a strong strain rate dependence to the deformation response, which qualitatively matches the experimental results obtained by Weeks and Sun [8].

2. Crashworthiness Simulation:

Crushing of a composite square tube is presented here. The material used here is E-Glass/Epoxy laminated composite with [30°/-30°] fiber orientation. (Note: E-glass fibers are assumed to be rate independent here). The material properties for the example are listed in Tables 3-5. The inelastic properties given in Table 4 were determined by Goldberg [1] for a toughened epoxy. For purposes of this example, identical properties were used here. The composite tube is assumed to be fixed at one end and impacted by a rigid wall at the other end. The strain rate of the simulation is 40/sec. Material Model 58 of the nonlinear explicit finite element code LS-DYNA is also used to simulate the crash behavior of the tube. Model 58 is one of the composite material models provided by LS-DYNA library. This material model is rate independent. Comparison is performed for the predicted results of the presented methodology, the experimental data and the simulation results using material Model 58 in LS-DYNA [9]. Material properties used in Model 58 are presented in Table 6.

Figure 10 shows the initial condition of the square composite tube meshed with shell elements. In this case, the full integration shell element is used to simulate the crash of the tube. Figure 11 shows the shape of the tube 10ms after impact when the displacement of the rigid wall reaches 100mm. Figure 12 shows the comparison of rigid wall force (reaction forces) of present model, material model 58, and experimental data. It can be observed that the result of the present model fits the experimental data well. Furthermore, the results demonstrate that incorporating nonlinearity and strain rate dependence into the composite material model can significantly improve the quality of the analytical predictions.

3. Perforation Simulation:

The developed material model is examined in hypervelocity impact simulation of armors. Solid finite element is employed in the simulation. This example is considered to demonstrate the capability of the model to simulate such a phenomenon. There is no experimental validation for this simulation and it is purely illustrative. It also demonstrate the stability of the developed formulation is such simulations. The plate is made of AS/PEEK with properties as listed in Tables 1 and 2. The impactor is a Tungsten bar with initial velocity of 1 Km/sec. The eroding contact algorithm in LSDYNA is utilized in the simulation. This contact algorithm is an adaptive contact, which is activated when failure occurs. Figure 13 depicts the results of the simulation at two instants of time (3.5 micro-seconds and 5.0 micro-seconds).

Table-1 Material Properties of AS-4 Fiber Tows:

	Longitudinal Modulus (Gpa)	Trans Modulus (Gpa)	In-plane Shear Modulus (Gpa)	Out of Plane Shear Modulus (Gpa)	In-plane Poisson's Ratio	Out of Plane Poisson's Ratio
Symbol	E_L	E_T	G_{LT}	G_{TT}	ν_{LT}	ν_{TT}
Value	214.0	14.0	14.0	14.0	0.2	0.2

Table-2 Material Properties of PEEK resin:

E_m (Gpa)	G_m (Gpa)	ν	D_0 (1/sec)	n	Z_0 (Mpa)	q	Ω_m (Mpa)	β
4.0	1.42	0.4	1.0E+4	0.7	630	310	52	0.45

Table-3 Material Properties for Unidirectional E-glass Fiber

	Longitudinal Modulus (Gpa)	Trans Modulus (Gpa)	In-plane Shear Modulus (Gpa)	Out of Plane Shear Modulus (Gpa)	In-plane Poisson's Ratio	Out of Plane Poisson's Ratio	Failure allowable (Gpa)
Symbol	E_L	E_T	G_{LT}	G_{TT}	ν_{LT}	ν_{TT}	X_{tf}
Value	41.40	3.381	5.244	5.244	0.0244	0.3	0.7866

Table-4 Material Properties of Epoxy resin

	Young's Modulus (Gpa)	Shear Modulus (Gpa)	Poisson's Ratio	Tensile Strength (Gpa)	Compressive Strength (Gpa)	Shear Strength (Gpa)
Symbol	E_m	G_m	ν_m	Y_{tm}	Y_{cm}	S_m
Value	3.45	1.3	0.35	0.1911	0.1911	0.05382

Table-5 Inelastic Material Properties of Epoxy resin:

Symbol	D_0 (1/sec)	n	Z_0 (Mpa)	q	Ω_m (Mpa)	β
Value	1.0E+4	0.5	1030	160	69	0.45

Geometry parameters:
Length of the tube = 254 mm
Cross-section = 50.8×50.8 mm
Thickness = 1.829 mm
Radius of the corner = 0.0 mm
Density = 1.8 gm/cm^3
Velocity of the rigid wall = 10 mm/ms

Table-6 Material Properties Used In Model 58 of LSDYNA

	Gpa	Gpa	Gpa			
Symbol	E_a	E_b	E_c	V_{ba}	X_t	X_c
Value	41.4	3.381	3.381	0.0244	0.7866	0.7866
Symbol	G_{ab}	G_{bc}	G_{ca}	Y_t	Y_c	S_c
Value	5.244	5.244	5.244	0.1911	0.1911	0.05382
Symbol	ε_{11c}	ε_{11t}	ε_{22c}	ε_{22t}	ε_{gms}	
Value	0.019	0.019	0.056	0.056	0.011	

Discussion and Conclusion

Strain rate dependent constitutive equations based on the state variable method are formulated to model the rate-dependent deformation response of the polymer matrix. A micromechanics based model which includes the strain rate dependent behavior of the matrix is developed for unidirectional fiber reinforced polymer matrix composite materials. The deformation model has been implemented into an explicit dynamic finite element code LS-DYNA, used for simulating the behavior of composite structures under various loads such as impact and tensile loading. Within the model a representative volume cell is assumed. The effective stresses in the unit cell were computed given the effective strains. Micro Failure Criterion (MFC) is presented for each material constituent and failure mode. Examples of composite materials under crash and tensile loading are used to validate the model. The predicted results compared well to experimentally obtained stress-strain curves.

Acknowledgements

Computational resources in this research is provided by The Ohio Supercomputer Center. Their support is gratefully appreciated.

References

1. Goldberg, R., "Strain Rate Dependent Deformation and Strength Modeling of a Polymer Matrix Composite Utilizing a Micromechanics Approach", NASA/TM-1999-209768, 1999.
2. Tabiei, A. and Chen, Q., "Micromechanics Based Composite Material Model for Impact and Crashworthiness Explicit Finite Element Simulation", J. of Thermo-Plastic Composites, 14: (4), pp. 264-289, 2001.
3. Stouffer, D.C. and Dame, L.T., "Inelastic Deformation of Metals: Models, Mechanical Properties and Metallurgy", John Wiley and Sons, New York, 1996.
4. Bordonaro, C., "Rate Dependent Mechanical Behavior of High Strength Plastics: Experiment and Modeling." Ph.D. Dissertation, Rensselaer Polytechnic Institute, Troy, New York, 1995.
5. Goldberg, R., "Implementation of Fiber Substructuring Into Strain Rate Dependent Micromechanics Analysis of Polymer Matrix Composites", NASA/TM-2001-210822, 2001.
6. Tabiei, A., Jiang, Y., and Simitses, G. J., "Compressive Behavior of Moderately Thick Plates With Progressive Damage", Mechanics of Composite Materials and Structures, Vol. 4, pp. 281-295, 1997.
7. Hahn, H. T. and Williams J. G., "Compression Failure Mechanisms in Unidirectional Composites", Composite Materials: Testing and Design, ASTM STP 893, 1986, pp. 115-139.
8. Weeks, C., and Sun, C., "Nonlinear Rate Dependence of Thick-Section Composite Laminates." High Strain Rate Effects on Polymer, Metal and Ceramic Matrix Composites and Other Advanced Materials, AS-Vol. 48, Y.D.S. Rajapakse and J.R. Vinson, eds., ASME, pp. 81-95, 1995.
9. LSTC, "LSDYNA users manual, version 960", Livermore, CA, 2001.

Figure 1. A Representative Unit Cell of Unidirectional Fiber Reinforced Composite

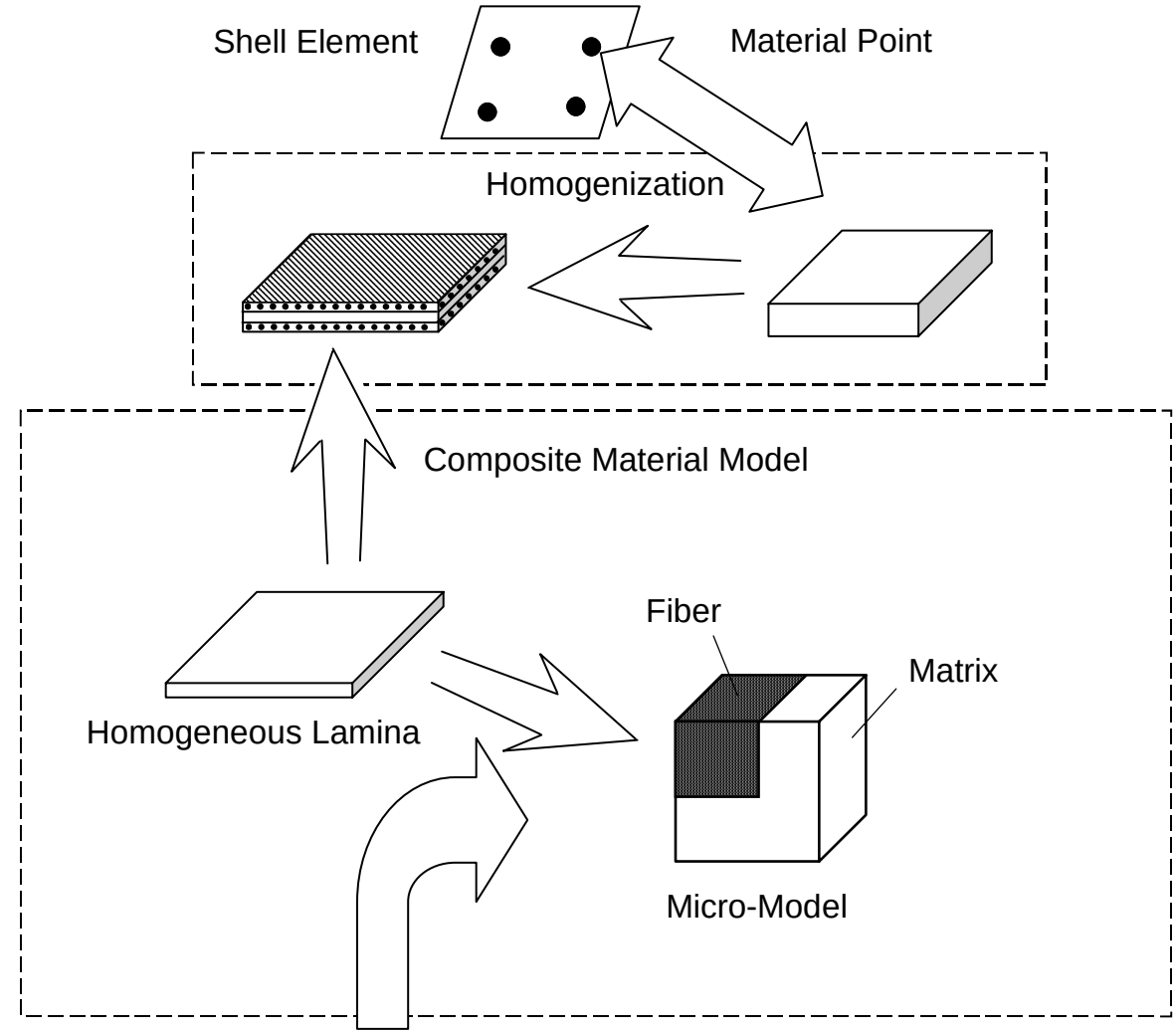

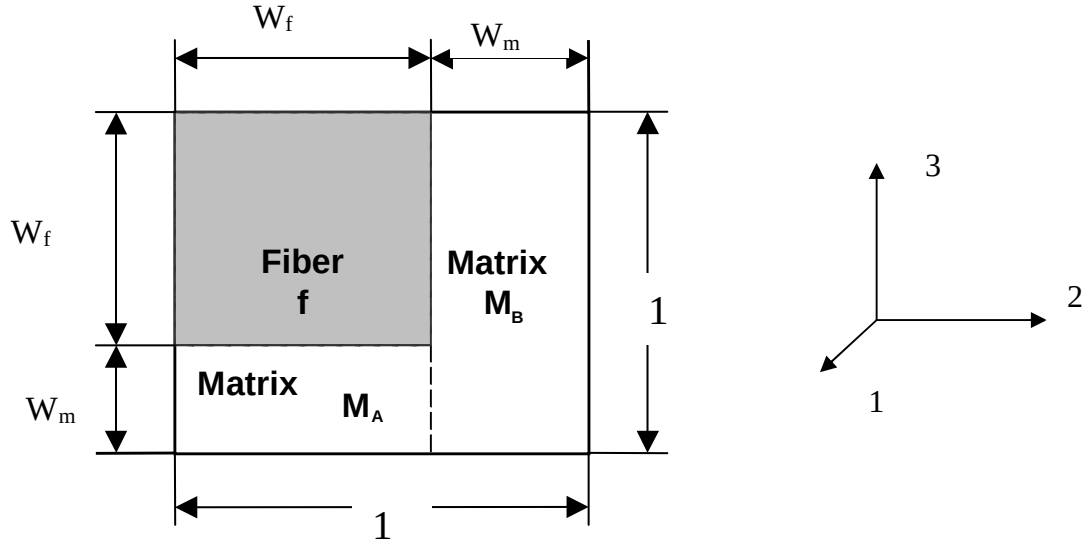

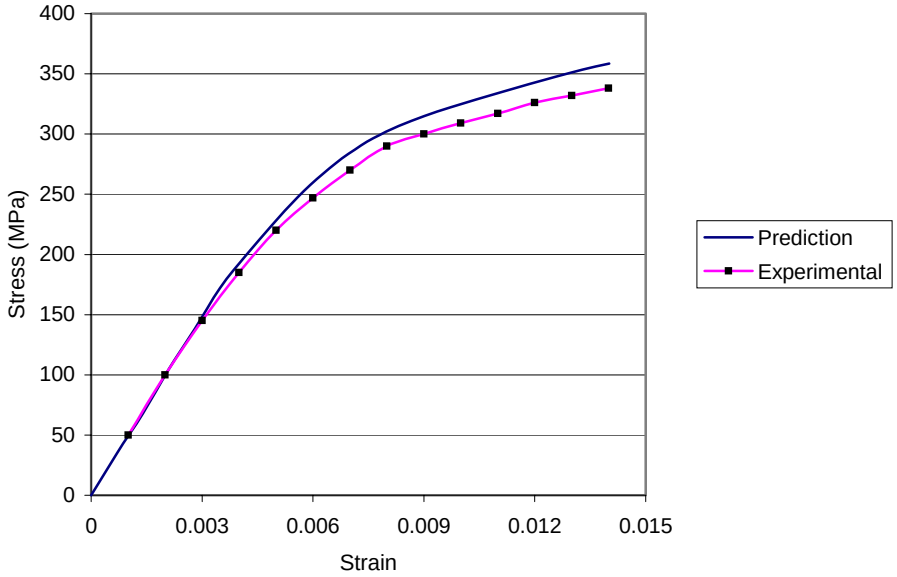

Figure 2. Comparison of Prediction and Experimental Data for [15°] AS4/PEEK at the Strain Rate of 0.1/sec (Shell Elements)

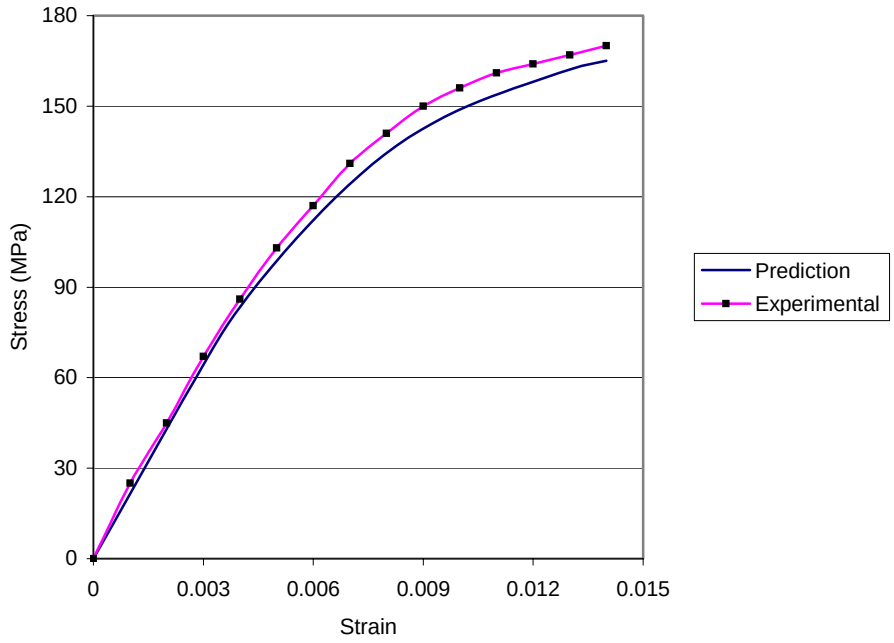

Figure 3. Comparison of Prediction and Experimental Data for [30°] AS4/PEEK at the strain rate of 0.1/sec (Shell Elements)

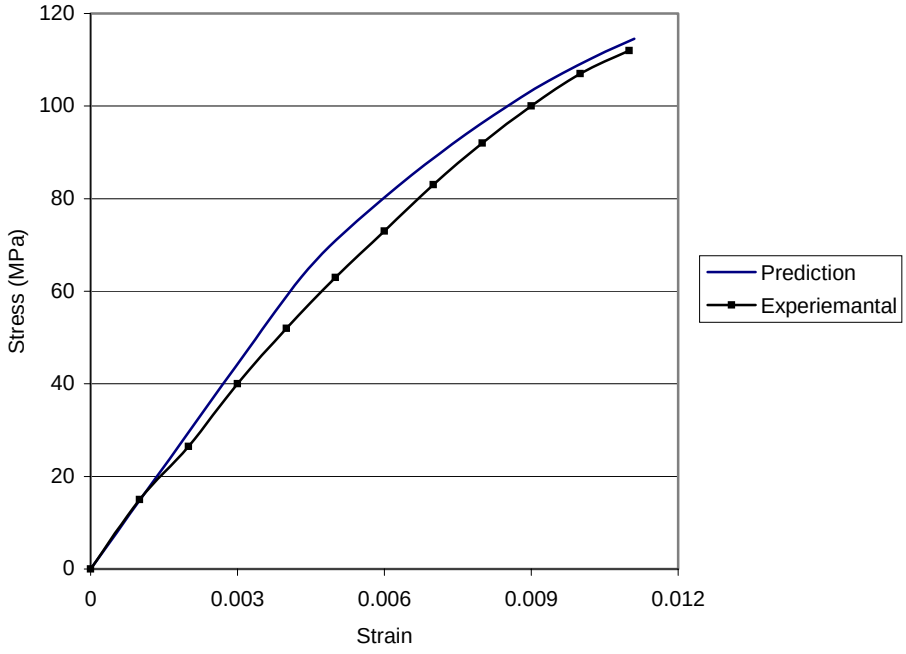

Figure 4. Comparison of Prediction and Experimental Data for [45°] AS4/PEEK at the Strain Rate of 0.1/sec (Shell Elements)

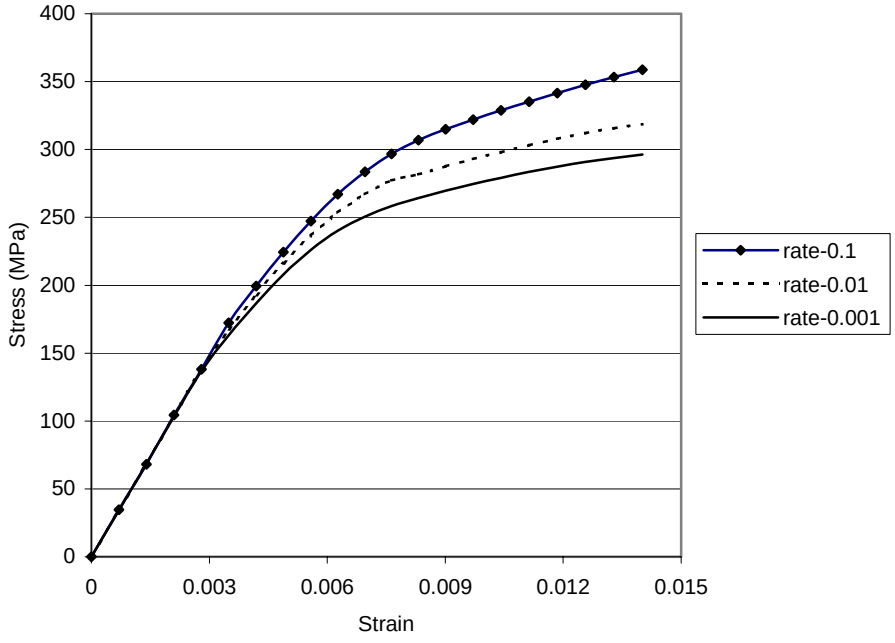

Figure 5. Predictions of [15°] AS4/PEEK at Different Strain Rates (Shell Elements)

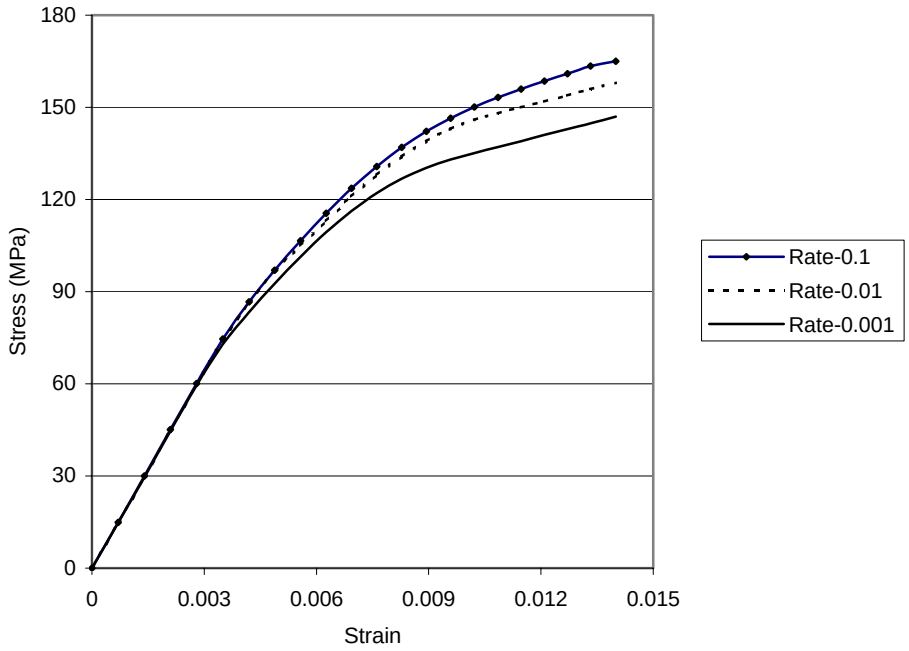

Figure 6. Predictions of [30°] AS4/PEEK at different Strain Rates (Shell Elements)

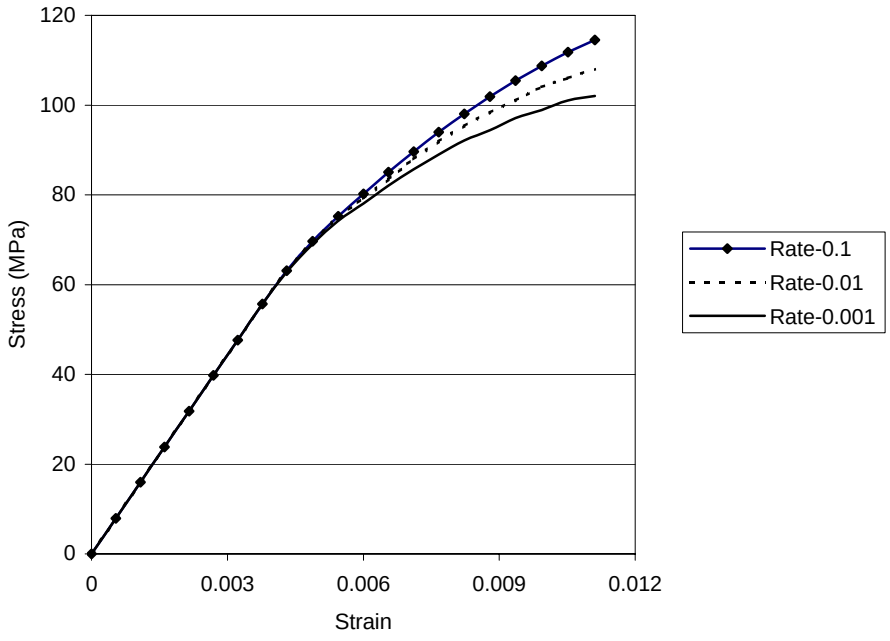

Figure 7. Predictions of [45°] AS4/PEEK at different Strain Rates (Shell Elements)

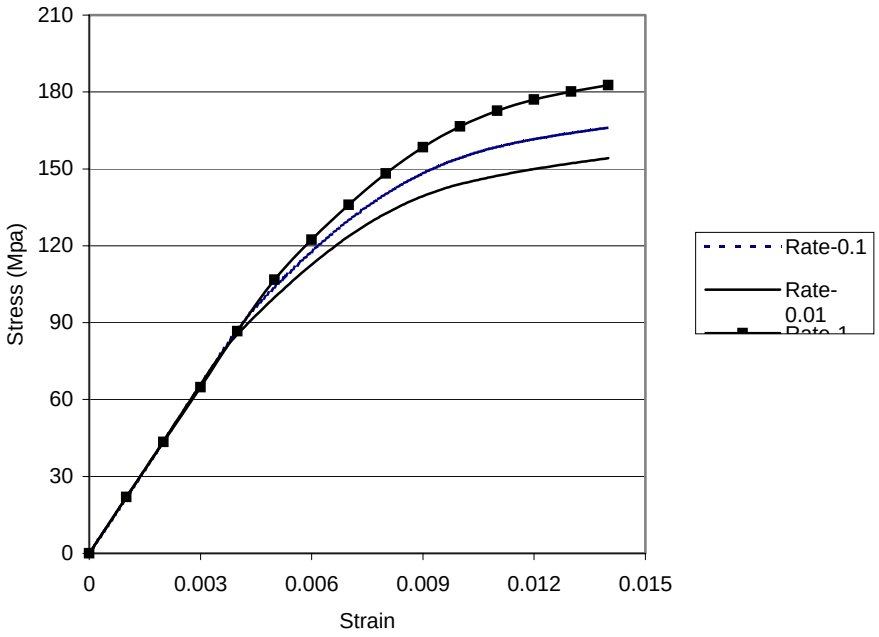

Figure 8. Prediction of [30°] AS4/PEEK at Different Strain Rate (Solid Elements)

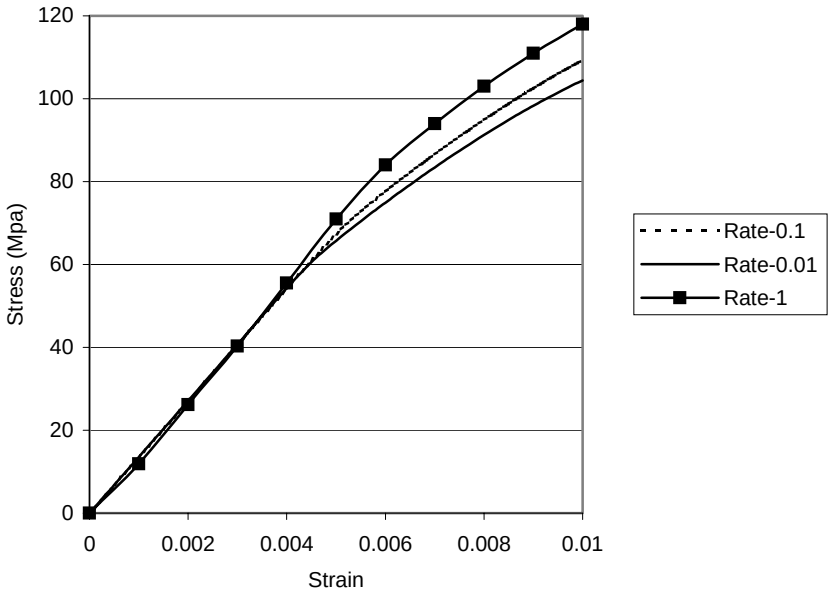

Figure 9. Prediction of [45°] AS4/PEEK at Different Strain Rate (Solid Elements)

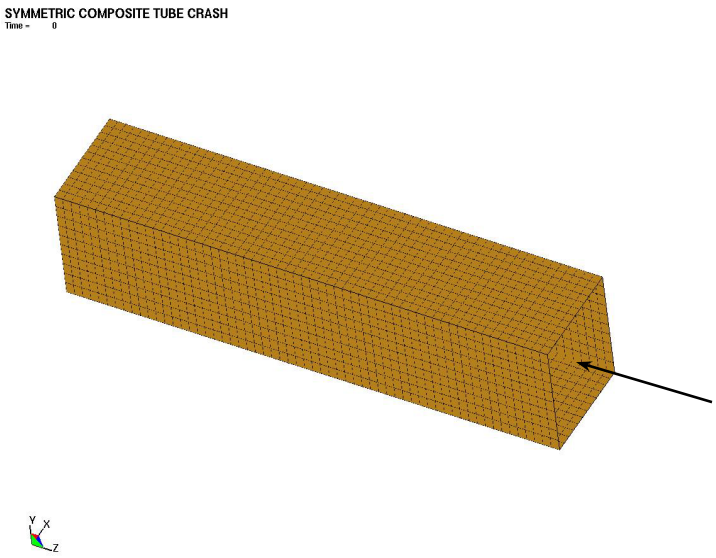

Figure 10. Composite Tube [30°/-30°] at Initial Condition

Figure 11. Composite Tube [30°/-30°] Under Impact (after 10ms)

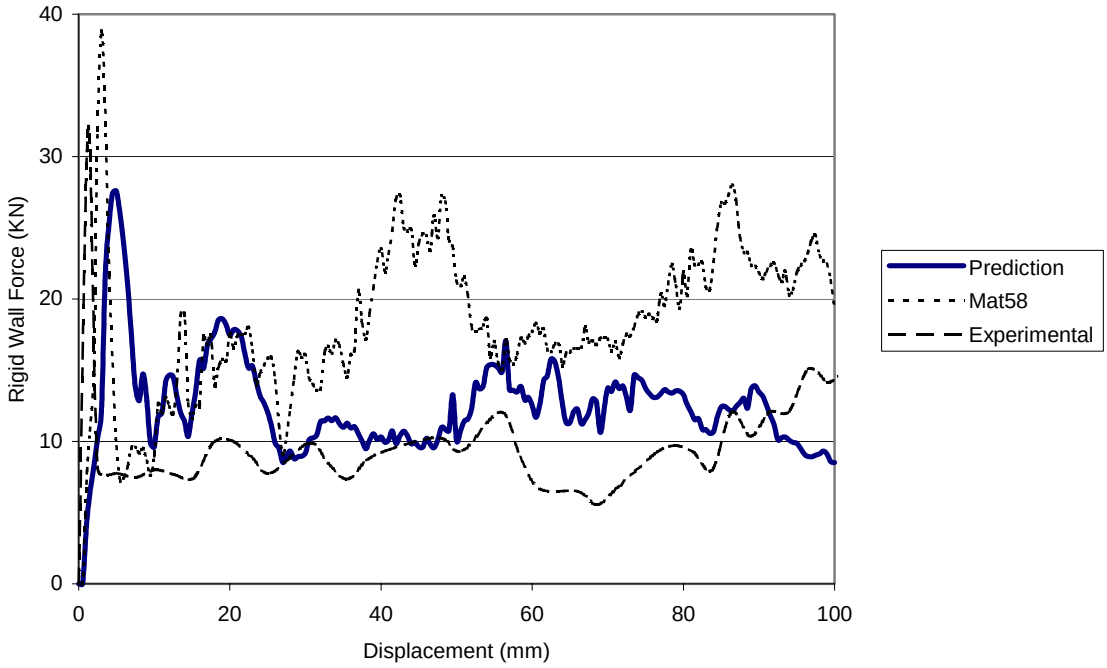

Figure 12. Comparison of Present model, Experimental Data, and Result of Mat 58 for Eglass/Epoxy Composite Tube Crash

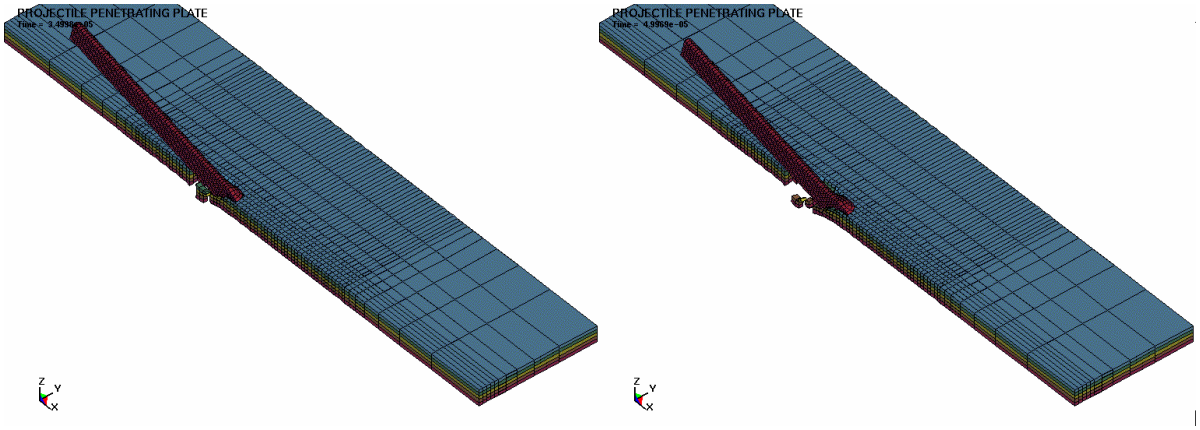

Figure 13. Perforation prediction of strain rate dependent armor plate